

# Theory and Application of Sonoelasticity Imaging

L. Gao,<sup>1</sup> K. J. Parker,<sup>1</sup> S. K. Alam,<sup>1</sup> D. Rubens,<sup>2</sup> R. M. Lerner<sup>3</sup>

<sup>1</sup>Department of Electrical Engineering and Rochester Center for Biomedical Ultrasound, University of Rochester, Rochester, NY 14627

<sup>2</sup>Department of Radiology and Rochester Center for Biomedical Ultrasound, University of Rochester, Rochester, NY 14627

<sup>3</sup>Department of Diagnostic Radiology, Rochester General Hospital, Rochester, NY 14621

Received 19 June 1996; revised 6 August 1996

**ABSTRACT:** Sonoelasticity imaging uses low-frequency (100-Hz) vibrations in tissue and Doppler imaging of vibration patterns to detect and define hard tumors. Fundamental theoretical considerations of sonoelasticity imaging are reviewed in this article, to predict the image of a small hard tumor in a background of softer elastic tissue. Comparisons from experimental work on elastic phantoms and from finite element analyses confirm the ability of vibration images to define small inhomogeneities. © 1997 John Wiley & Sons, Inc. *Int J Imaging Syst Technol*, **8**, 104–109, 1997

**Key words:** doppler; elasticity; vibration; imaging; shear waves

## I. INTRODUCTION

Sonoelasticity is a rapidly evolving medical imaging technique for visualizing hard tumors in tissues. In this novel diagnostic technique, a low-frequency vibration is externally applied to excite internal vibrations within the tissue under inspection. A small stiff inhomogeneity in surrounding tissue appears as a disturbance in the normal vibration eigenmode pattern. The low-frequency vibrations in deep tissue can be detected using Doppler ultrasound. By employing a properly designed scanning and detection algorithm, a real-time vibration image can be made. For a comprehensive review of the subject, please refer to Ophir et al. [1] and Gao et al. [2].

## II. THEORY

We model a tumor as an elastic inhomogeneity inside a lossy homogeneous elastic medium. For example, the media stiffness is a constant  $E_o$ , except the small area around  $(x_o, y_o)$  has the stiffness  $E_o + E'$ . When we apply boundary conditions and a driving vibration force on the medium, we want to compare the vibration patterns of this medium with and without the inhomogeneity.

For simplicity, we will consider the two-dimensional case.

Since low-frequency longitudinal waves have wavelengths that are too large compared with organs of interest at the frequencies used in sonoelasticity imaging [3], we have chosen to concentrate on shear waves. The shear wave equation for a general linear and isotropic material is [4]:

$$\nabla^2 \xi - \frac{1}{C^2} \frac{\partial^2 \xi}{\partial t^2} = 0 \quad (1)$$

where the shear wave velocity  $C$  is given by:

$$C = \left( \frac{E}{2\rho(1 + \nu)} \right)^{1/2} \quad (2)$$

If we define a special function  $\gamma(\vec{\mathbf{x}})$ , which is nonzero only in the tumor region, we can write one equation for the whole medium:

$$C^2(\vec{\mathbf{x}}) = C_o^2[1 + \gamma(\vec{\mathbf{x}})] \quad (3)$$

where  $C_o$  is the shear wave velocity in the homogeneous area. So instead of writing two equations for both the homogeneous and the inhomogeneous region, we may write one equation for the entire medium:

$$\nabla^2 \xi - \frac{1}{C_o^2(1 + \gamma(\vec{\mathbf{x}}))} \frac{\partial^2 \xi}{\partial t^2} = 0 \quad (4)$$

Including a relaxation term to account for losses [5], and with the assumption of the sinusoidal time dependence  $\xi = \xi \exp(i\omega_o t)$ , the equation above becomes:

Correspondence to: K. J. Parker

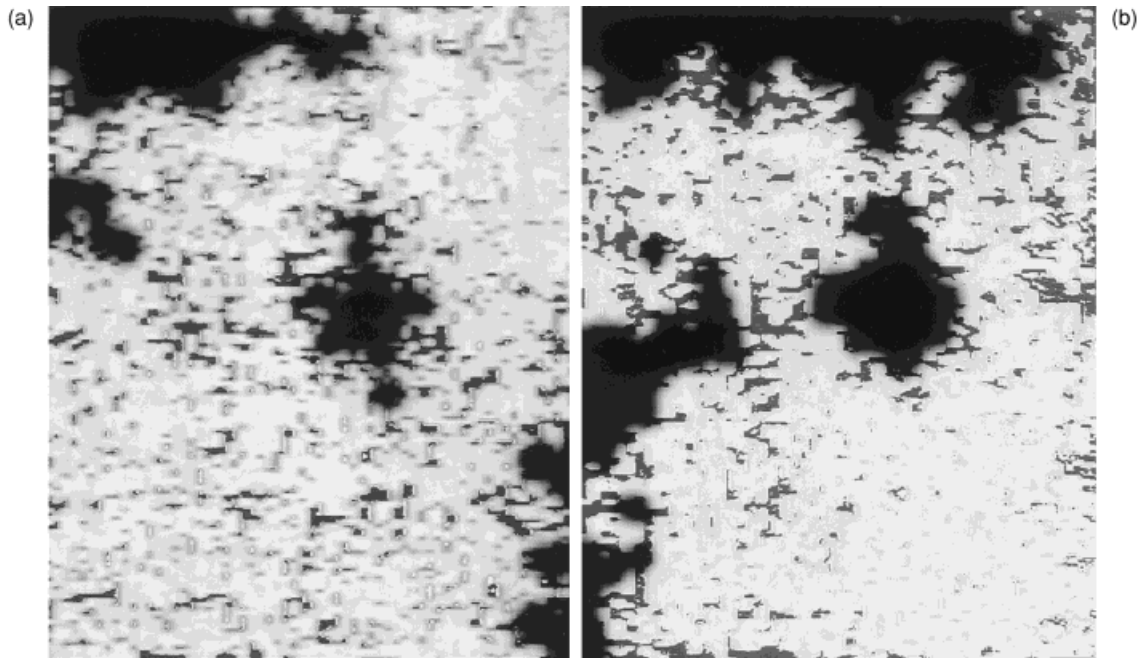


**Figure 1.** Inhomogeneous phantom vibration pattern. The source vibration is located on the right-hand side of the images. The inhomogeneity is located on the middle upper part of the images, which shows little or no vibration (black area). Source vibration frequency is (a) 37 and (b) 201 Hz.

$$\nabla^2 \xi + \frac{K^2}{[1 + \gamma(\vec{x})]} \xi - \frac{iK^2}{Q_o[1 + \gamma(\vec{x})]} \xi = 0 \quad (5)$$

There is no direct and closed form solution to the inhomogeneous

wave Equation (5). To find the solution, we can split the total wave into incident and scattered wave:

$$\xi = \xi_i + \xi_s \quad (6)$$

The incident wave satisfies the homogeneous wave equation,

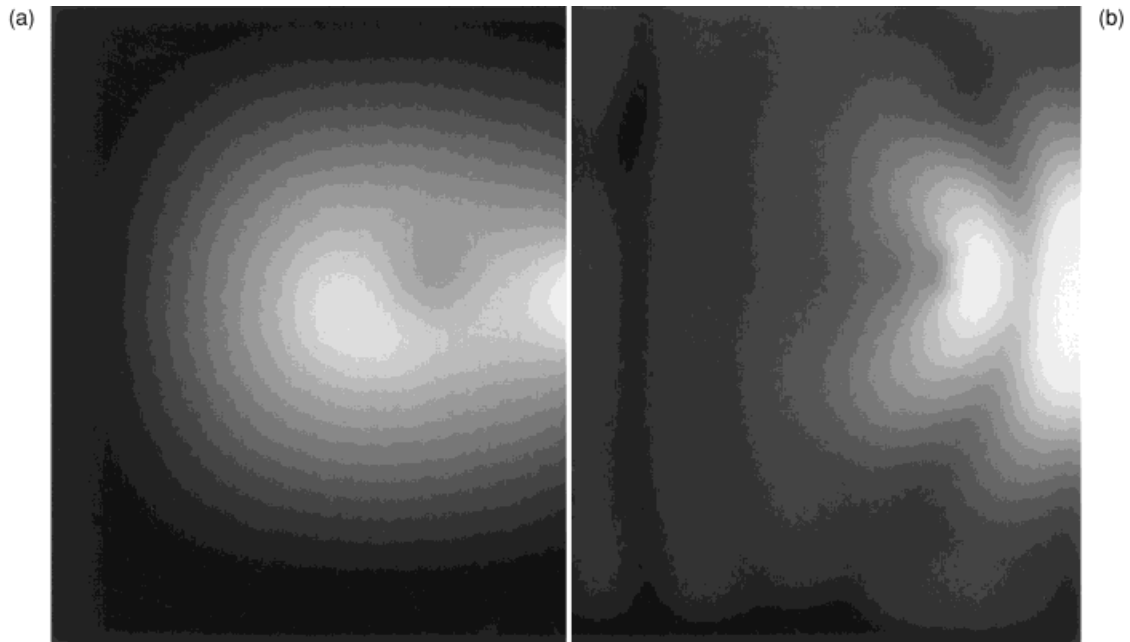


**Figure 2.** Theoretical inhomogeneous vibration pattern. The source vibration is located on the right-hand side of the images. The inhomogeneity is located on the middle upper part of the images, which shows little or no vibration (black area). Source vibration frequency is (a) 37 and (b) 201 Hz.

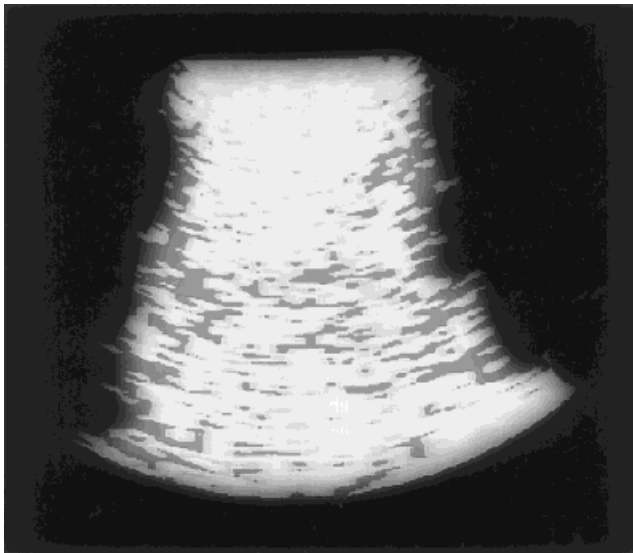


**Figure 3.** Liver scan experiment. The orientation of the scan is such that the anterior abdominal muscles are located at the top of the image, the diaphragm at the bottom. Image shows only regions of vibration within the right lobe of a normal liver.

which can be solved with a given set of boundary conditions. The scattered wave due to the inhomogeneity satisfies the following equation:

$$\nabla^2 \xi_s + K^2 \xi_s - \frac{iK^2}{Q_0} \xi_s = \beta(\vec{\mathbf{x}})(\xi_i + \xi_s) \quad (7)$$

where  $\beta(\vec{\mathbf{x}})$  is a function of the tumor size, stiffness, and location. If the tumor is small, we may assume that the scattered wave is much smaller than the incident wave and discard the term  $\beta(\vec{\mathbf{x}})\xi_s$  on the right-hand side. (This is analogous to the Born approximation for longitudinal wave scattering [6].) The inhomogeneous equation can thus be solved. The final solution is given by a sum of an infinite series for the cost of a regular two-dimensional geometry with prescribed boundary conditions as given by Gao et al. [7,8].

### III. EXPERIMENT

Phantom, *in vitro* and *in vivo* experiments were conducted to study the possibility of tumor detection by sonoelasticity. The real time images on the Acuson 128XP scanner are conventional B-scan images, but with the addition of specially modified green-scale overlay. The brightness of the green-scale is proportional to the amplitude of the vibration. For printing reproducibility, we converted the green images to black and white images for all the experimental results shown with normal B-scan speckle suppressed (lowered to dark gray values). Thus, the brightness of the gray-scale is proportional to the amplitude of the vibration.

Since the theory given above is two dimensional, we constructed long rectangular phantoms. The dimension of the phantom was about  $5 \times 5 \times 30$  cm (width  $\times$  height  $\times$  length). Two kinds of experiments were conducted. The first employed a homogeneous phantom; the second included an inhomogeneity.

The homogeneous phantom was constructed using 500 g of water, 500 g of ethylene glycol, 70 g of gelatin, 100 g of glycerol, 100 g of formalin, and 10 g of barium sulfate. A gel phantom (1.5% agar, 1.5% gelatin, 0.1% barium sulfate) was used for the second experiment. A harder gel tube (3% agar, 3% gelatin, 0.1% barium sulfate) was buried in the phantom as the inhomogeneity. The Young's modulus of the hard gel tube was about four times that of the phantom. The diameter of the hard gel tube was 0.6 cm.

The inhomogeneous phantom experiment result is shown in Figure 1. A vibration was applied from the right hand side of the image. The experiment shown in Figure 1(a) and 1(b) used 37 and 201 Hz vibration, respectively. Notice the black middle upper part is just where the inhomogeneity was located. The corresponding theoretical simulation images using solutions to Equation (7) and parameters matched to the phantom [8] are shown in Figure 2. The inhomogeneity appears as dark region, which indicates low vibration amplitude. The vibration pattern is similar to that in Figure 1.

For the *in vivo* liver experiment, a low-frequency vibration (about 20 Hz) was conducted into a volunteer's liver (informed consent had been obtained from the volunteer). The vibration image inside the liver is shown in Figure 3, and the corresponding theoretical simulation is shown in Figure 4. The vibration source was applied near the top of the images. Although the simulation neglects the layered abdominal wall, the irregular liver shape, and ill-posed boundaries, comparing the results with Figure 3, the patterns are similar and display simple modal patterns that are indicative of vibration within a relatively homogeneous medium.

Some *in vivo* prostate experiments were performed by conducting vibration along the transrectal probe and by activating Doppler color detection of vibration. Figure 5(a) is a B-scan image showing homogeneous structure. Figure 5(b) is the corresponding sonoelasticity image showing a decreased vibration in one region, which was later determined by guided biopsy and pathology to be a tumor present in that location.

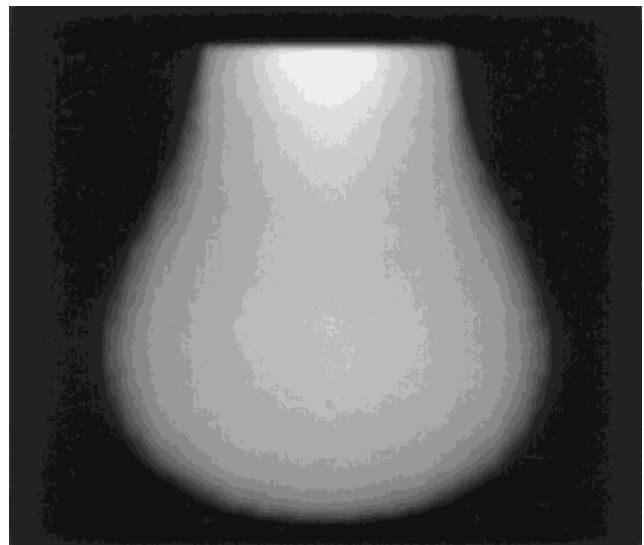


**Figure 4.** Liver scan simulation using our theory for a homogeneous, bounded medium with a Gaussian vibration source.

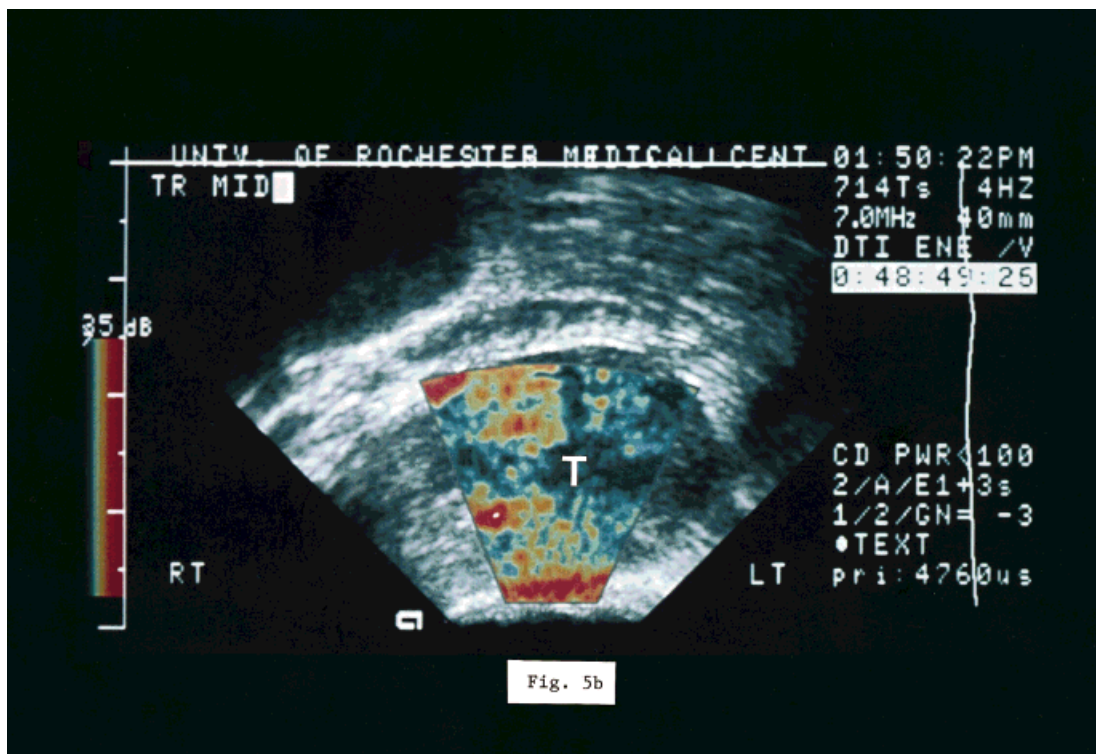


**Figure 5.** (a) Transverse, midsection B-scan of a prostate with equivocal gray-scale echogenicity. (b) Real-time, in vivo sonoelasticity image of the same prostate as in (a). Color is displayed in regions with greater vibration amplitude. A tumor (T) is delineated and depicted as a void in the vibration pattern.

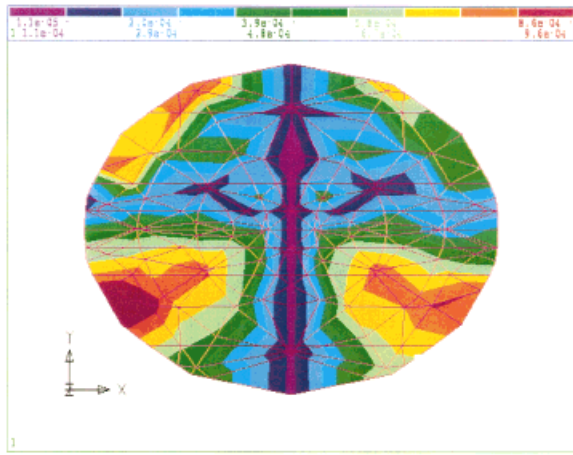


Fig. 6 -ho-S-h without tumor, sagittal view, h-direction motion

**Figure 6.** Finite element analysis of a prostate, without tumor, undergoing small vibrations, sagittal view, x-direction motion.

#### IV. FINITE ELEMENT ANALYSIS

Finite element analysis tools can further verify the theory. It can also help to study the behavior of tissue vibration under more complicated situations, such as irregular boundary conditions, irregular geometry of the object, and irregular shape of the inhomogeneity.

We employed an elliptical sphere as a model for the prostate. NASTRAN (McNeill-Schwindler) was used for the analysis. The maximum length of the  $x$ -axis was 6 cm, that of  $y$ -axis was 4.8 cm, and that of  $z$ -axis was 4 cm, which were close to the average size of the prostate. It is also divided into different parts with different Young's modulus [7]. About 2000 tetra elements were used, and boundary conditions were established to mimic the pelvic cavity structures.

The simulation results with an excitation frequency of 100

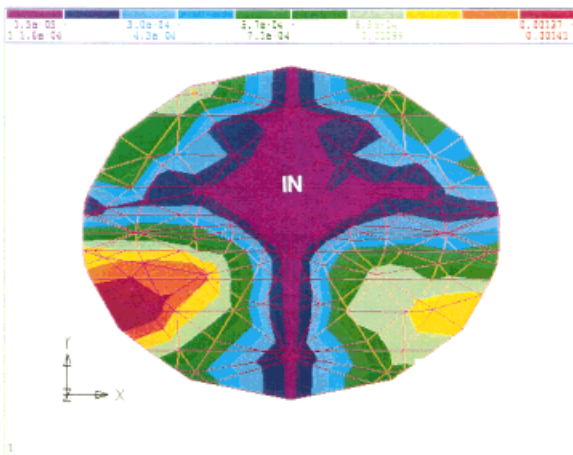
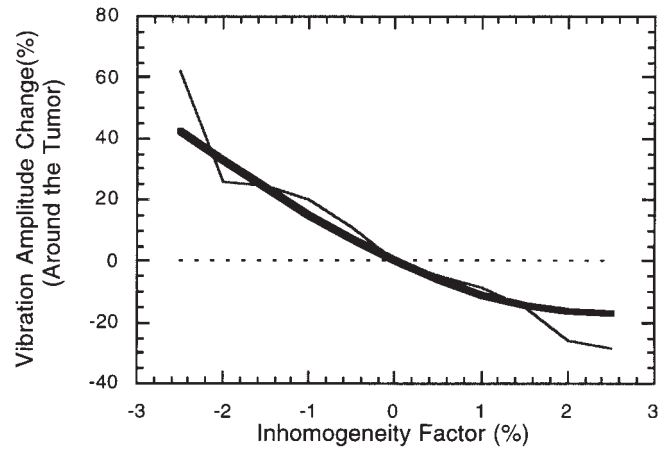


Fig. 7 -in-S-h with tumor, sagittal view, h-direction motion. Notice the tumor (upper middle region) has made the vibration amplitude around it lower, compared with the previous figure

**Figure 7.** With tumor, sagittal view, x-direction motion. Notice the tumor (upper middle region) has made the vibration amplitude around it lower, compared with the previous figure.



**Figure 8.** Vibration-amplitude curve due to inhomogeneity. The thick solid curve is from theory, and the thin one is from finite element analysis. They show very good correspondence. (The dash line was drawn to show the zero base line.)

Hz (typically used in the clinical trial) are presented in Figures 6 and 7. Figure 6 is the case without a tumor, showing the sagittal view of the vibration along  $x$  axis. Figure 7 shows a corresponding pattern with a tumor. We can see that the tumor lowered the vibration significantly around it. (In the figures, red represents the highest vibration amplitude; then it decreases as magenta, yellow, green, etc. Blue and violet represent the lowest amplitude. Usually there is about one to two orders of magnitude difference between the highest and the lowest amplitude.) Thus, the basic prediction of the previous theory can be also applied to the complicated prostate system for *in vivo* study; that is, we should look for the low-vibration amplitude regions for hard tumors.

We further compared the predictions of our theory and that of finite element analysis. Specifically, we quantified the change in vibration amplitude resulting from a tumor. Our approach is to vary the area and stiffness of the lesion, and compare the localized vibration amplitude change due to the inclusion, as predicted by the finite element analysis and the theory. To do this, we modeled the  $5 \times 5 \times 30$ -cm phantom described previously by both finite element analysis and by our elastic-Born approximation. The elastic properties of the inhomogeneous tumor were varied.

The results from the theory and the finite element analysis correspond very well (Fig. 8). As expected, the larger the absolute value was of the inhomogeneity factor, the larger was the vibration amplitude change. A hard lesion produces vibration amplitude drop, and interestingly, a soft lesion produces a vibration amplitude increase. The slope of the curve increases when the vibration frequency increases, but the basic characteristics discussed above stay the same. These results indicate that smaller hard inhomogeneities may be better discriminated at higher-vibration frequencies. However, in practice, greater losses limit the upper range of useful vibration frequencies, such that in practice frequencies below 200 Hz are commonly used.

## V. CONCLUSION

Sonoelasticity imaging was performed on phantoms, prostate in vitro, and liver in vivo. Results were compared against theoretical predictions. The theory was found to satisfactorily predict the essential features of sonoelasticity imaging. Finite element analysis was also employed to model vibrations inside tissue. The results corresponded well with our theoretical predictions. These results may be useful in optimizing vibration and imaging systems such that small, discrete, hard tumors can be routinely identified in clinical applications of sonoelasticity imaging.

## REFERENCES

1. J. Ophir, I. Cespedes, B. Garra, H. Ponnekanti, Y. Huang, and N. Maklad. "Elastography: Ultrasonic imaging of tissue strain and elastic modulus in vivo," *Eur. J. Ultrasound* **3**, 49–70 (1996).
2. L. Gao, K. J. Parker, R. M. Lerner, and S. F. Levinson. "Elastic imaging of tissue—a review," *Ultrasound Med. Biol.* **22**, 959–977 (1996).
3. K. J. Parker and R. M. Lerner. "Sonoelasticity of organs: Shear waves ring a bell," *J. Ultrasound Med.* **11**, 387–392 (1992).
4. L. D. Landau and E. M. Lifshitz, *Theory of Elasticity* (translated from the Russian by J. B. Sykes and W. H. Feid), (Pergamon Press Ltd., London), 1970, pp. 17–20.
5. L. E. Kinsler, A. R. Frey, A. B. Coppens, and J. V. Sanders, *Fundamentals of Acoustics* (Wiley, New York), 1982, pp. 90–91.
6. P. M. Morse and K. U. Ingard, *Theoretical Acoustics* (McGraw-Hill, New York), 1968, p. 413.
7. L. Gao, "Sonoelastography: Theory and experiment development," Ph.D thesis, University of Rochester, Rochester, NY, 1995.
8. L. Gao, K. J. Parker, S. K. Alam, and R. M. Lerner. "Sonoelasticity imaging: Theory and experimental verification," *J. Acoust. Soc. Am.* **97**, 3875–3886 (1995).